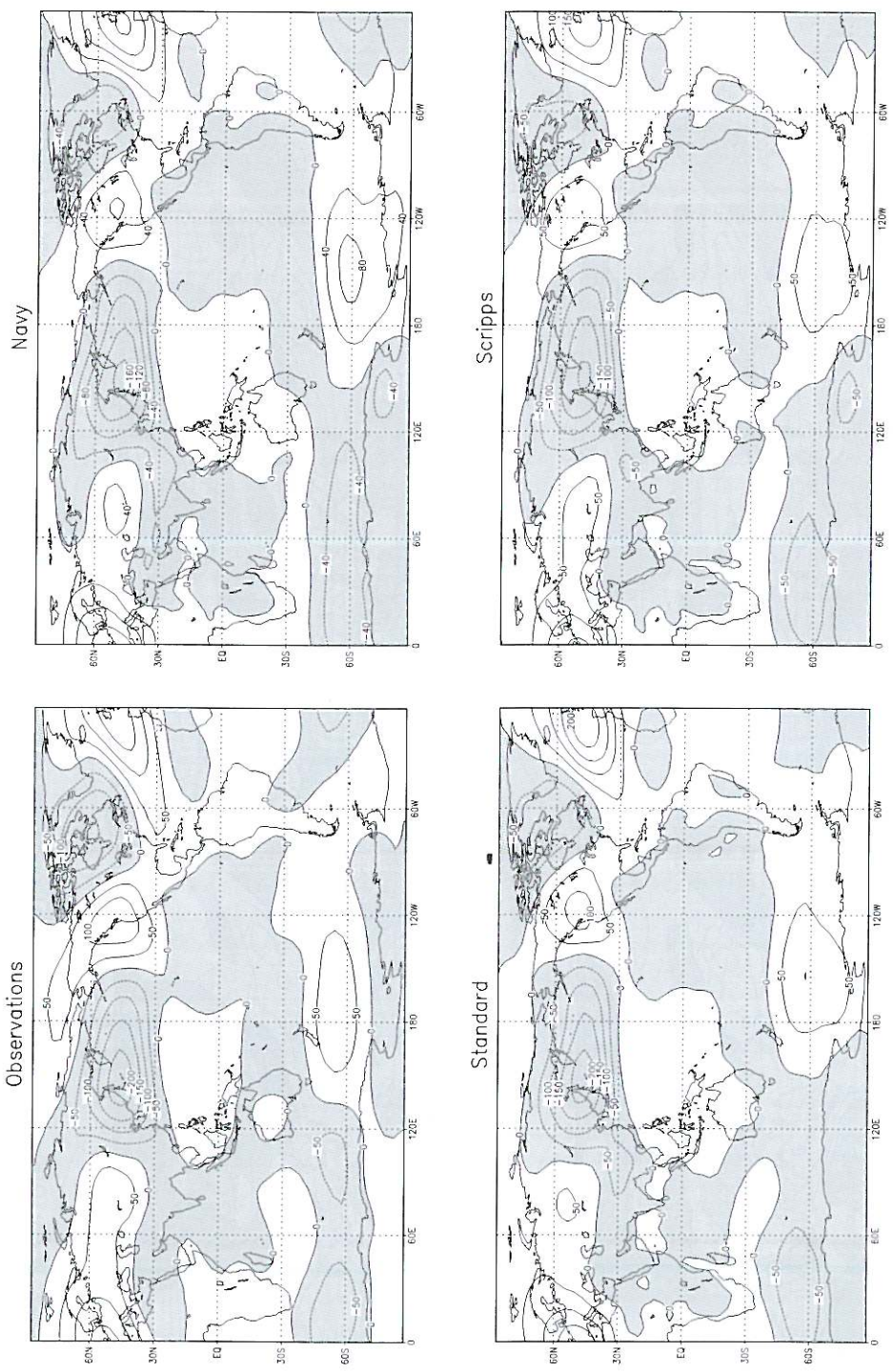

Fig. 13. Winter (DJF) geopotential height eddy filed at 500 mb for the observations (OBS), the Standard experiment, the Navy mountains data set and the Scripps mountains. Negative values are shaded. The contour is 40 m.

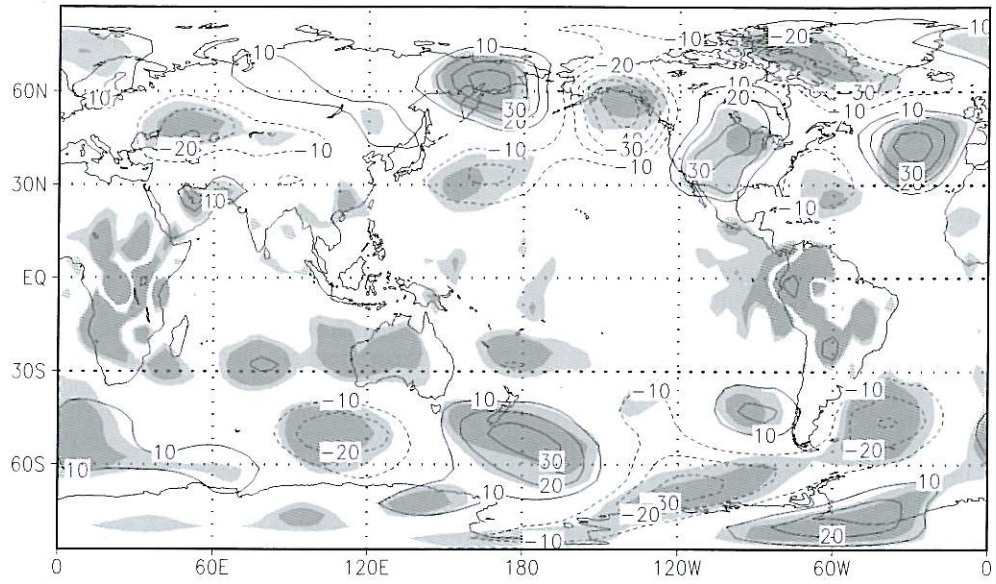

Fig. 14. Difference for winter (DJF) geopotential height eddy field at 500 mb between the Standard experiment and the Scripps mountains data set. Significance levels at 5% and 1% ar e shaded. The contour is 10 m.

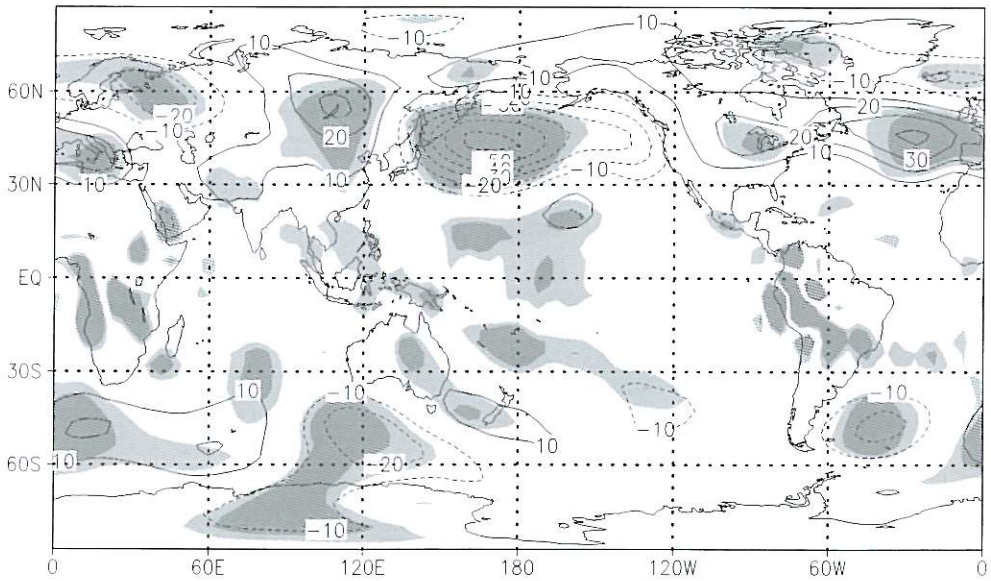

Fig. 15. Difference for winter (DJF) geopotential height eddy field at 500 mb between the Standard experiment, the Navy mountains data set. Significance levels at 5% and 1% are shaded. The contour is 10 m.

lies over Asia. The subtropical centers are reduced and brought more in accord with observation. The amplitude over Europe is reduced to 200 m from the 320 m of the Standard case. The overall reduction is substantial. The Scripps mountains (right bottom) generate a better wavetrain, that maintains some of the good points of the Navy data set (reduction of the European ridge), but with a smaller overall reduction of the anomalies strength. The centers of the wavetrain are not uniformly reduced and the response is relatively large scale compared to the mountain forcing (bottom panels of figs. 21 and 23).

A better appreciation of the differences in stationary waves can be obtained by looking at the difference fields. The new orographies (figs. 14 and 15) are both capable of reducing the amplitude over the Atlantic, as can also be seen from the difference between Navy and Scripps (fig. 16), showing no difference over the Atlantic and indicating a clear discrepancy over the Pacific. The Navy experiment reduces noticeably the amplitude over the North Pacific, whereas the effect is much weaker in the Scripps case. Overall, the comparison of the quality of the simulation of the large scale features of the general circulation aloft seems to be favorable to the Scripps case.

4.2. *Surface fields*

The precipitation shows a relatively smaller sensitivity, both in winter (fig. 18) and in summer (fig. 17). In the summer, in the Indian sector, a reduction of precipitation over the equatorial Indian Ocean is visible. The Scripps mountain experiment also shows a tendency to develop precipitation toward the Indian subcontinent, but overall the impact is relatively minor. Some beneficial impact is visible in Central America, where the excess precipitation over the south of Mexico is reduced, in accordance with observations. In winter, the reduction over the Indian Ocean is present in the Navy experiment, but not in the Scripps case. The Scripps experiment is improved in the Central Pacific where a larger reduction of the excess centers close to the dateline is achieved. The arid area in the Eastern Pacific is, however, better represented by the

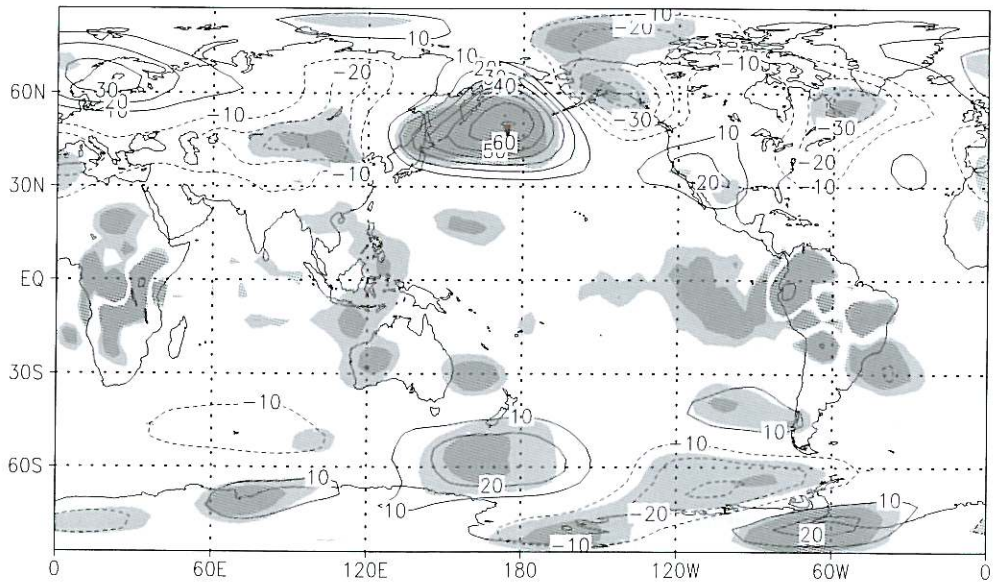

Fig. 16. Difference for winter (DJF) geopotential height eddy field at 500 mb between the Scripps experiment and the Navy mountains data set. Significance levels at 5% and 1% are shaded. The contour is 10 m.

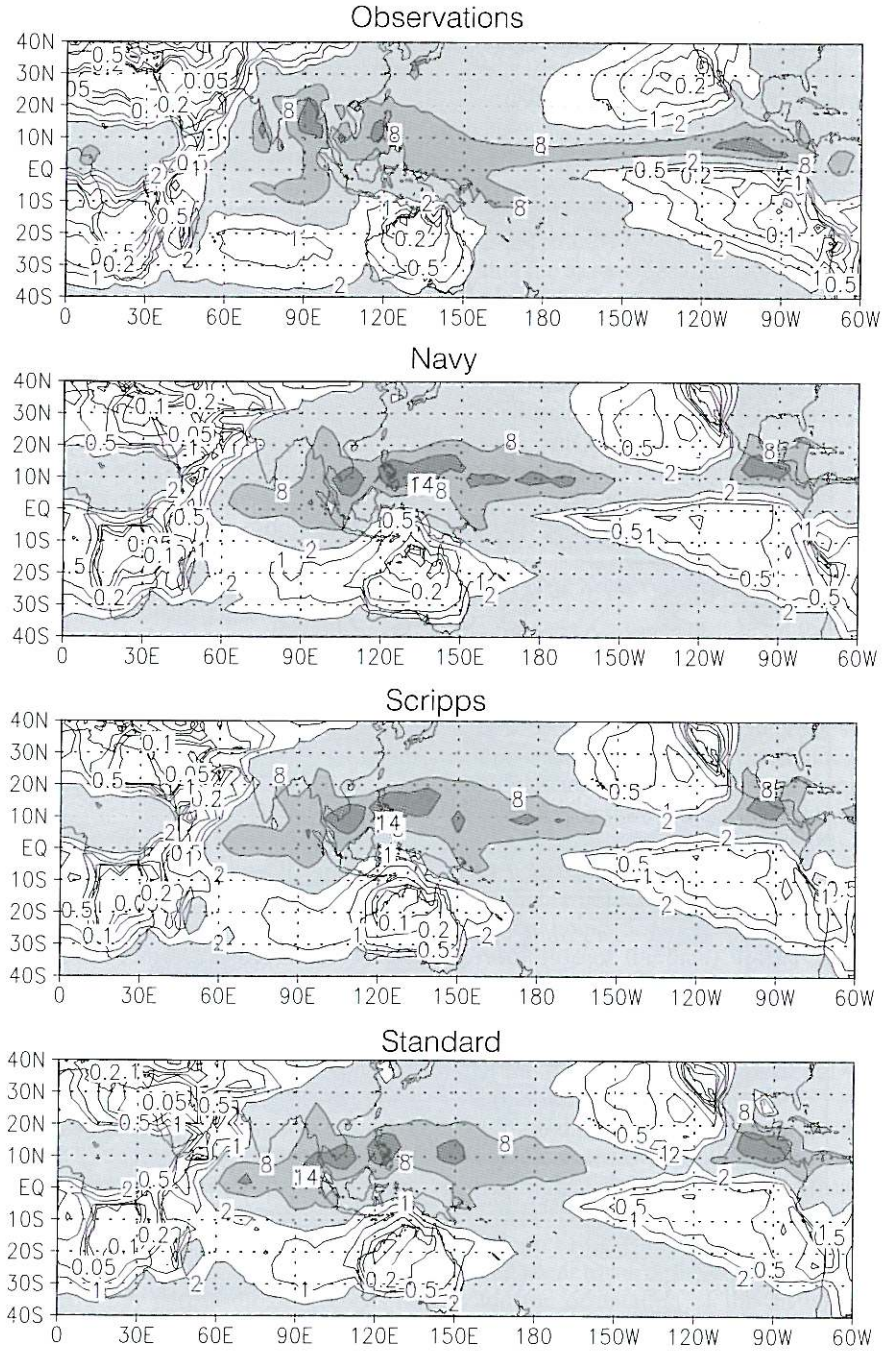

Fig. 17. Summer (JJA) precipitation for the observations (OBS), the Standard experiment (AMIP), the Navy mountains data set (AMIPNM) and the Scripps mountains (AMIPSC). The contour are in mm/day.

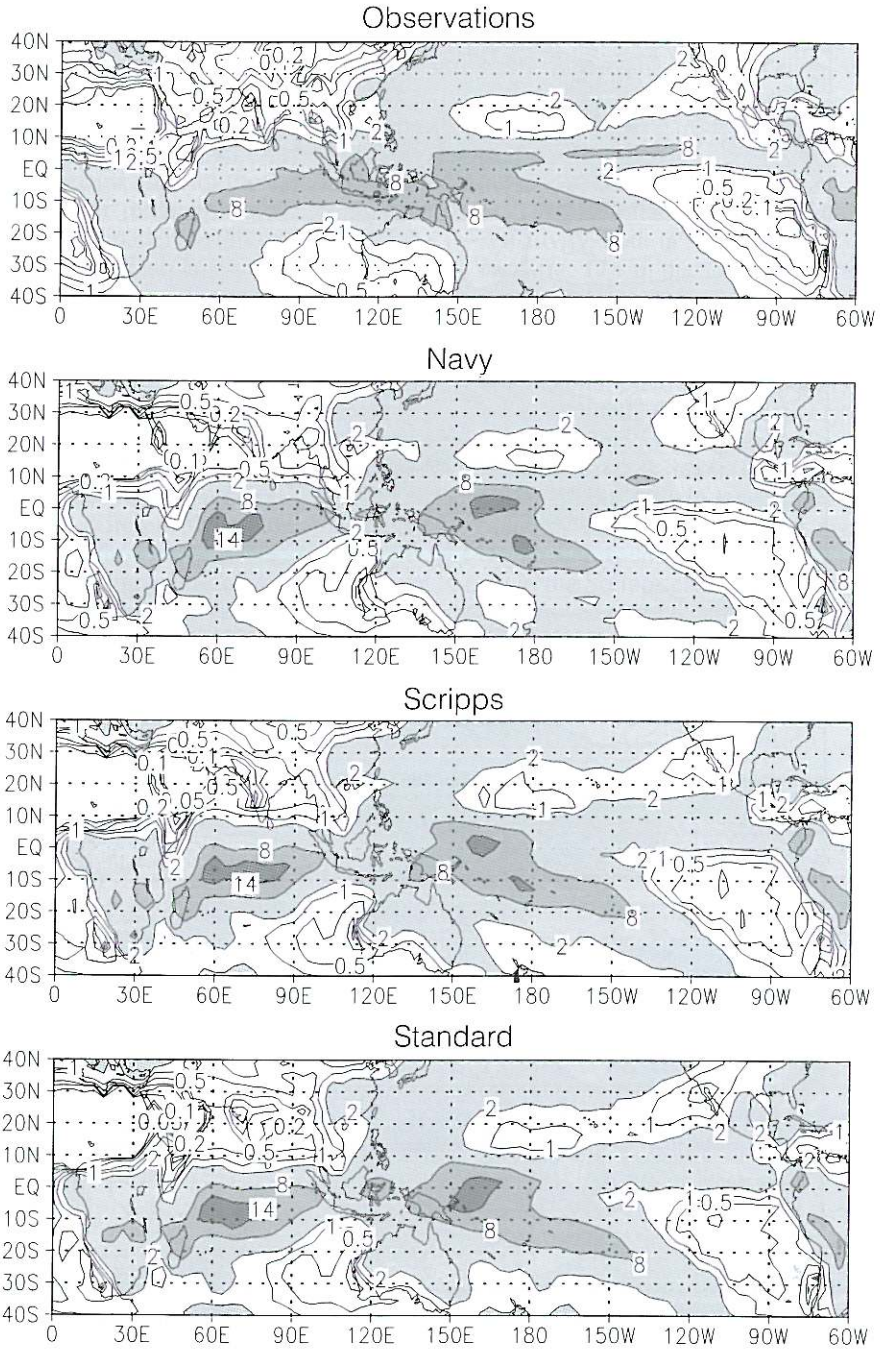

Fig. 18. Winter (DJF) precipitation for the observations (OBS), the Standard experiment (AMIP), the Navy mountains data set (AMIPNM) and the Scripps mountains (AMIPSC). The contour are in mm/day.

Navy mountains. The systematic error over the Indonesian archipelago, namely the break in the precipitation belt between 90E and 150E, does not show any improvement. It is very difficult to conclude which of the two mountain representations is superior. However, it is possible to see that the filtered mountains are both improved over the standard spectral mountains.

The global pattern of precipitation showed some indication that the precipitation in the Indian Ocean is affected. We can see the detail of the effect in figs. 19 and 20 that show in detail the Indian subcontinent area. The filters remove the fake elevation in the south of India and Southeast Asia. In both pictures the removal of the elevation around 10N results in a reduction of the precipitation over the equatorial Indian Ocean, a feature that is probably overestimated by the model. The small scale in the topography, that includes Gibbs oscillations, are not the only source of systematic error, but they certainly contribute to make the precipitation pattern worse. The strong correlation between the precipitation patterns and the local topography suggest that great care must be taken in consideration of this field.

4.3. *Evaporation*

The fields that are most closely linked to the properties of the surface may show the impact of orography more clearly, as the evaporation field (fig. 21). The global evaporation for Northern Hemisphere summer shown in fig. 22 shows the difference in the evaporation field for the Standard and Scripps experiments. The difference seems to be particularly large in the Pacific and in the Southern Atlantic and they can be traced to the differences between the mountains, mostly consisting of Gibbs oscillations. Large differences in the Indian Ocean can also be traced to the presence of a wavetrain of Gibbs oscillations in the Arabic Sea. A similar pattern emerged from the evaporation differences between the Navy and Standard experiment (fig. 23). In both cases the high spatial frequency part of the differences is highly correlated with the location of Gibbs oscillations, whereas the large scale differences are probably due to the differences in the large scale circulation. The oscillations appear to have a local effect on the evaporation, presumably through controlling the nominal height of the grid box, but the large scale changes in the midlatitudes are due to the change in the general circulation induced by the modifications in the stationary waves produced by the different mountains.

The organized character of the evaporation discrepancies caused by Gibbs-like oscillation is potentially a very cumbersome problem when that the atmospheric model is used as the atmospheric component of a coupled model. It is not difficult to imagine that the evaporation fields of the preceding picture will force a corresponding organized spurious pattern in the ocean with a potential generation of serious systematic errors. This is an important problem that needs to be considered more in detail in the formulation of coupled models.

4.4. *The Southern Eastern Pacific*

The area along the coast of Peru is a crucial area for the ENSO mechanism. The winds blowing along the coast produce intense upwelling that contributes to generate cold surface water that is advected towards the equatorial area. The along shore wind is present all through the year, with maximum intensity in the summer. The observations and the model results show the jet in a narrow region along the coast (the jet is probably in reality even closer to the coast, even if here it appears somewhat displaced due to the resolution of the data). In the Southern Hemisphere, Ekman pumping is to the left of the wind and in the South American coastal area this mechanism generates upwelling that is one of the sources of the surface cold water for the equatorial area in the north.

Standard topography generates in the Northern Hemisphere winter along shore wind of about the right density and with a remarkable good seasonal cycle, but the core is displaced by about 5 degrees longitude from its observed position. The shear towards the coast is in general weaker and the orientation of the jet is different. The results of these shortcomings is a situation that is not favorable to the presence of energetic upwelling in the area. The meridional wind stress shows similar signs in the same region. As an

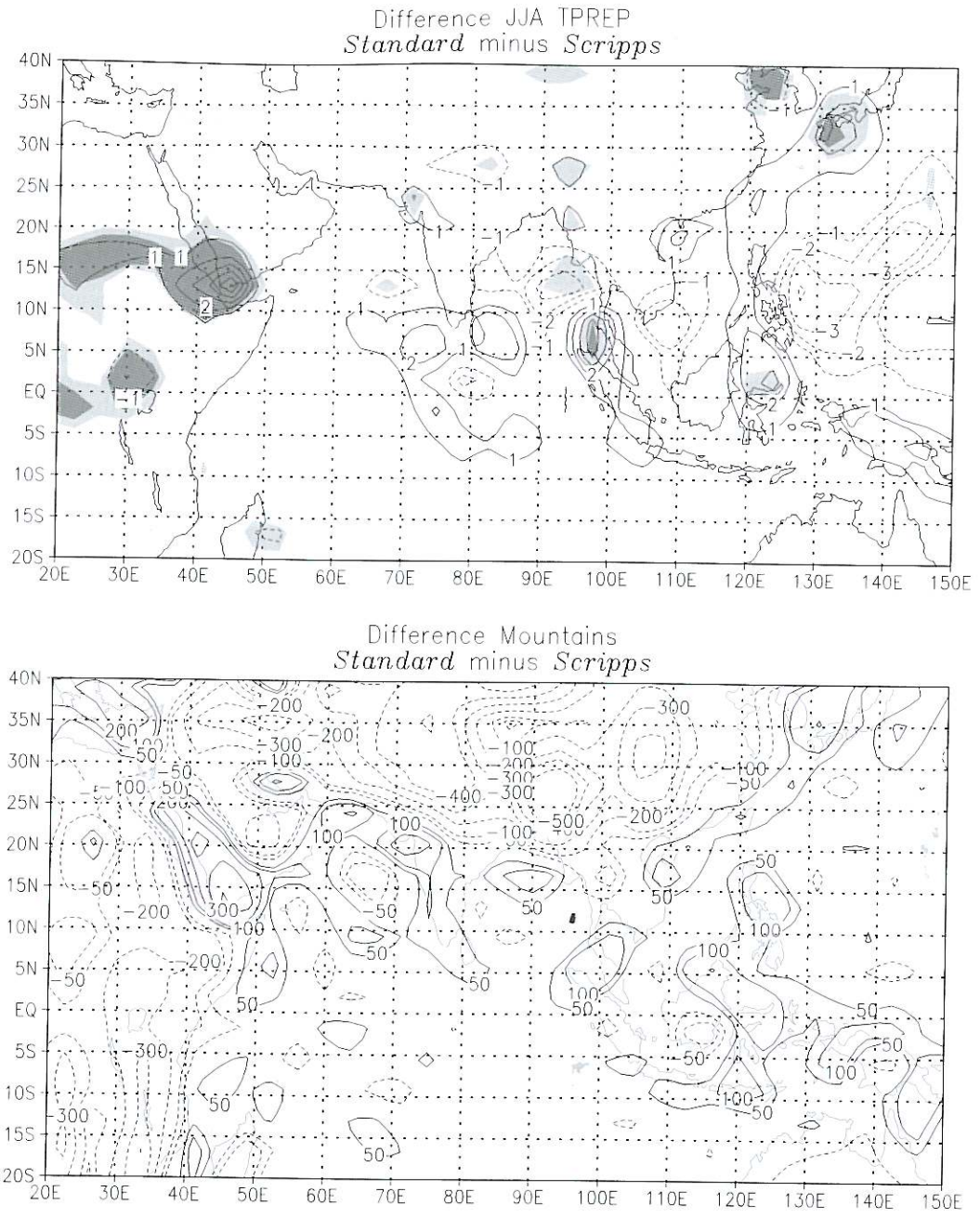

Fig. 19. Difference for summer (JJA) precipitation between the Standard experiment (011-AMIP) and the Scripps mountains experiment (012-AMIPSC). Significance levels at 5% and 1% are shaded. The contours are 1 mm/day in the top panel and every 100 m plus the contours at 50 m and −50 m in the bottom panel. Negative contours are dashed.

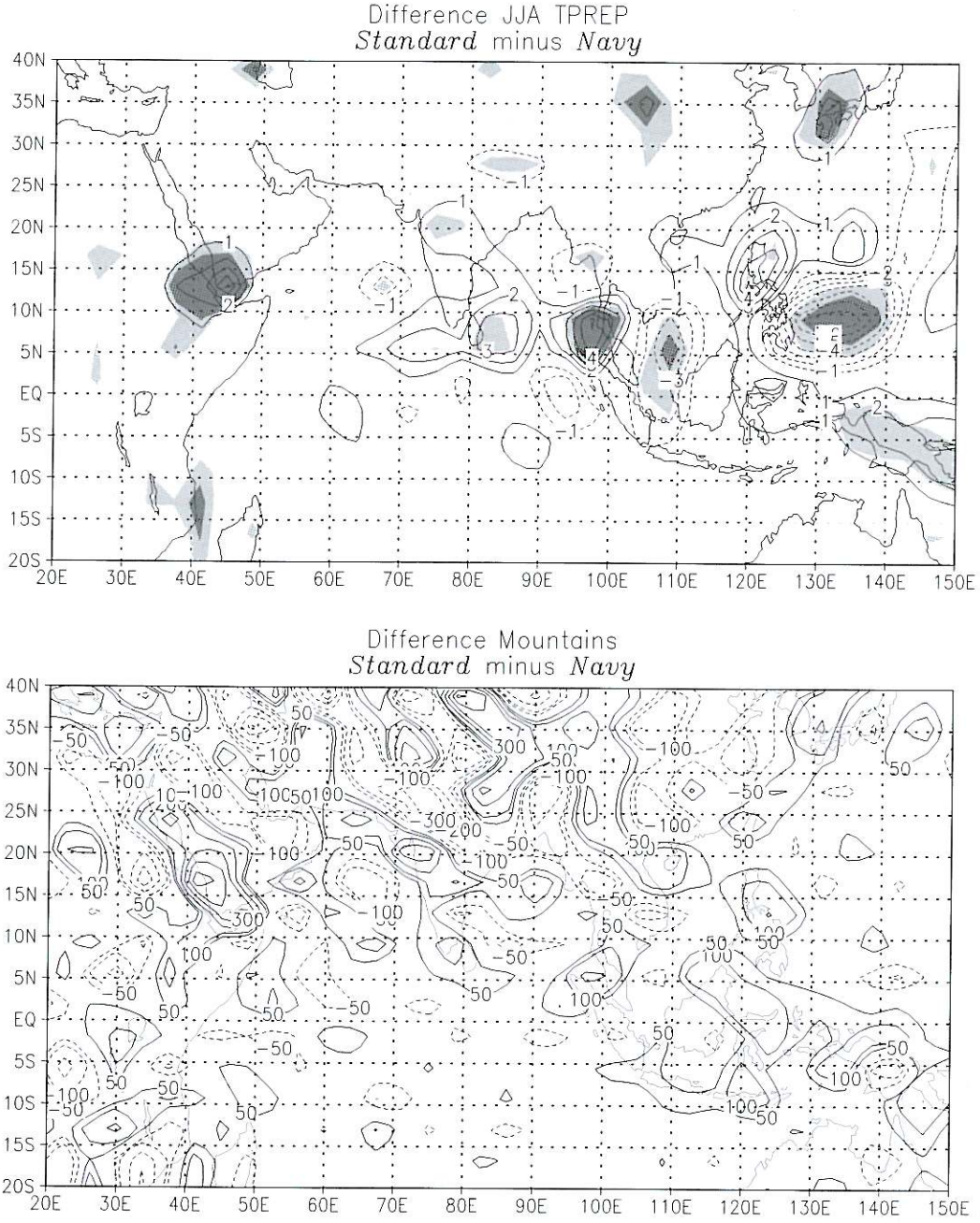

Fig. 20. Difference for summer (JJA) precipitation between the Standard experiment (011-AMIP) and the Navy mountains experiment (021-AMIPSC). Significance levels at 5% and 1% are shaded. The contours are 1 mm/day in the top panel and every 100 m plus the contours at 50 m and −50 m in the bottom panel. Negative contours are dashed.

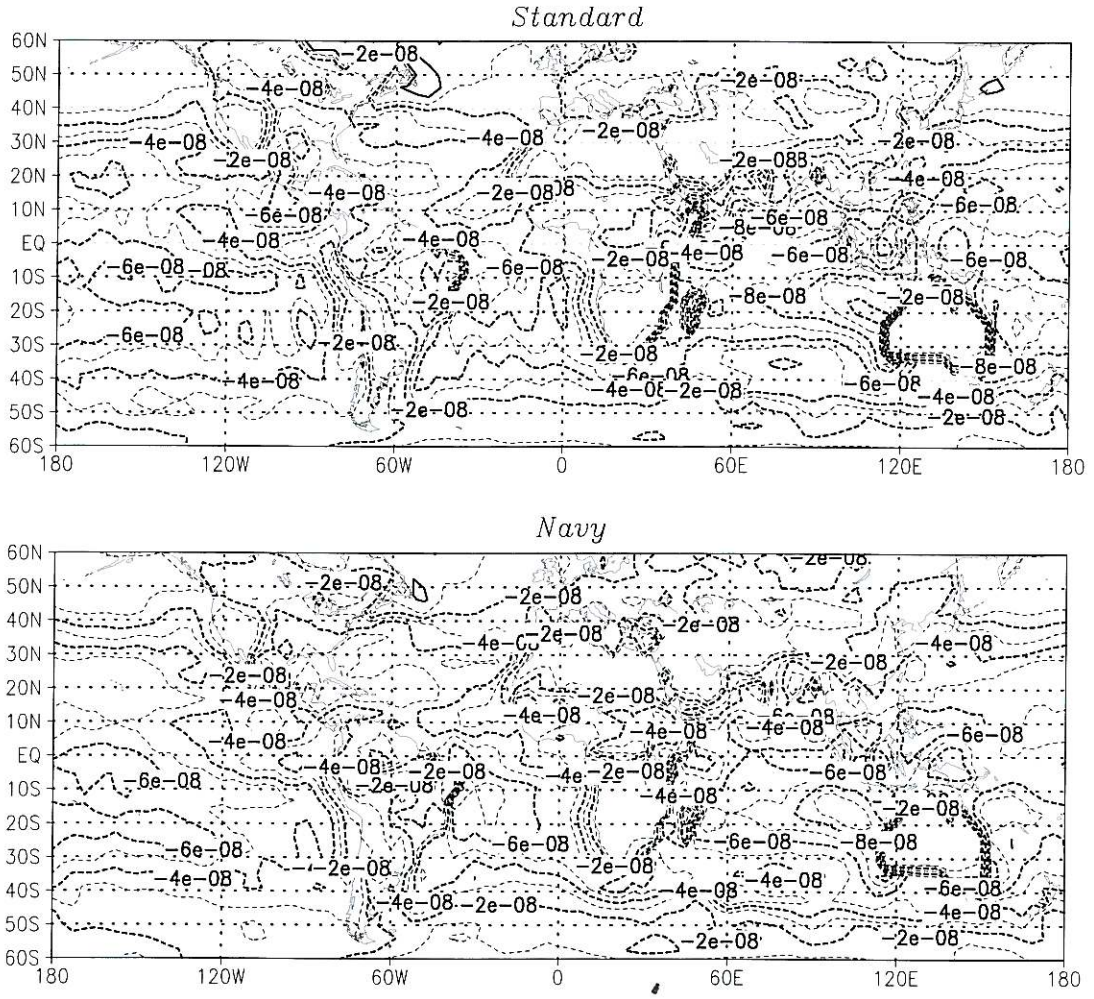

Fig. 21. Summer evaporation for the Standard and Navy experiments (bottom). The contour in the top panel is in kg/m^2 s.

example, we show in fig. 24 the differences between the Standard and the Navy experiments for the meridional wind stress. The shift of the Andes gradient and the elimination of the artificial archipelago in the Pacific contribute to push the surface stresses toward the Chilean coast. The differences are small and therefore we cannot conclude that we are obtaining a robust result, however it can be taken as an indication of the existence of a sensitivity in the area that needs further investigation.

5. Conclusions

A new filtering technique to eliminate Gibbs oscillations from the spectral model has been proposed. The method relies on the operational construction of a kernel that allows a very tight control on the filtering allowing an adaptive modulation of the filter strength and characteristic. The filter is applied to two mountains data set from different compilations of mountains for intermediate resolutions. The results of the

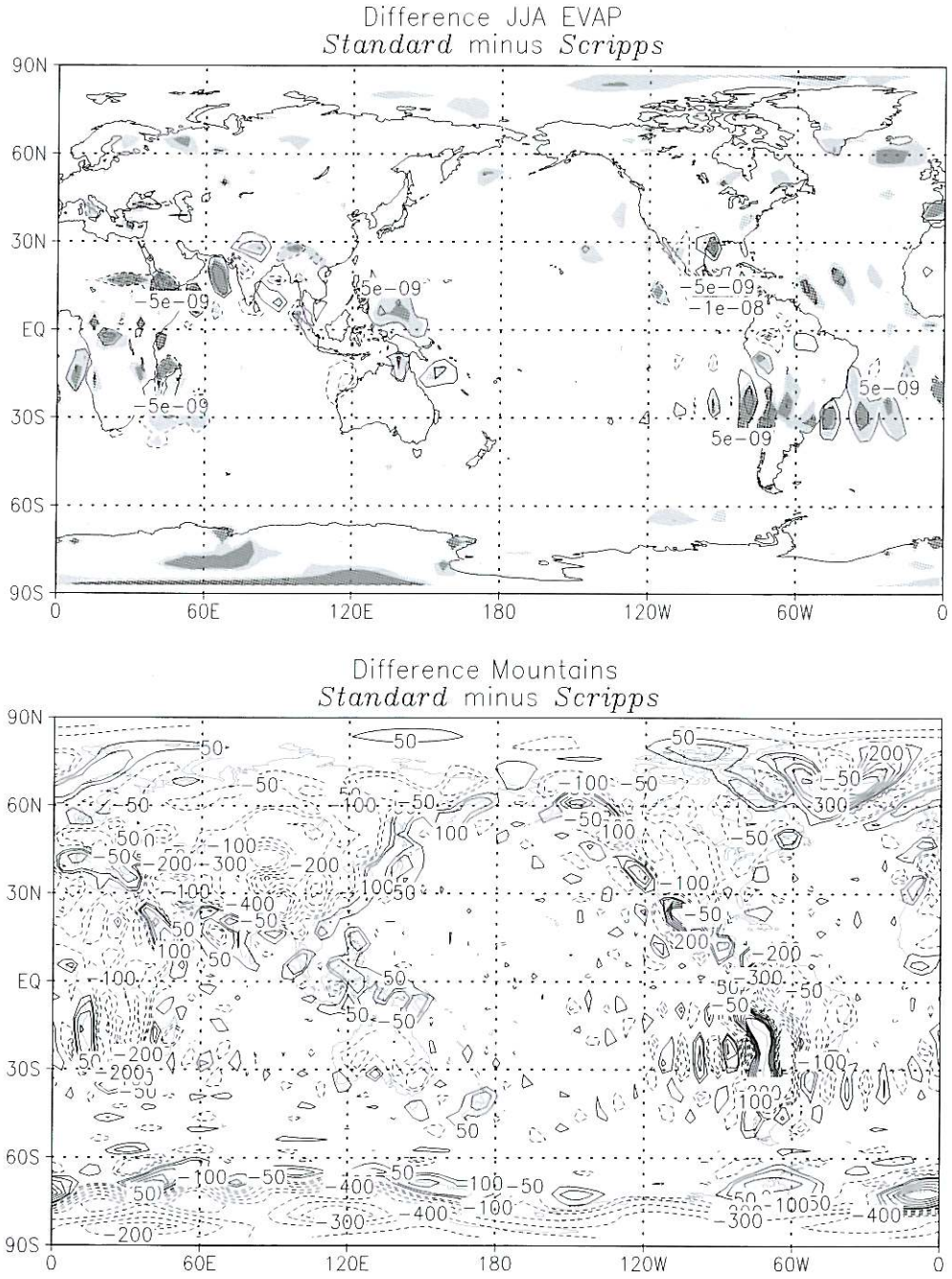

Fig. 22. Differences of evaporation between the Standard and Scripps experiments (top) compared to the differences in the topographies (bottom). Areas significant at 5% and 1% are shaded and the contour in the top panel is kg/m^2 s and every 100 m plus the contours at 50 m and −50 m in the bottom panel.

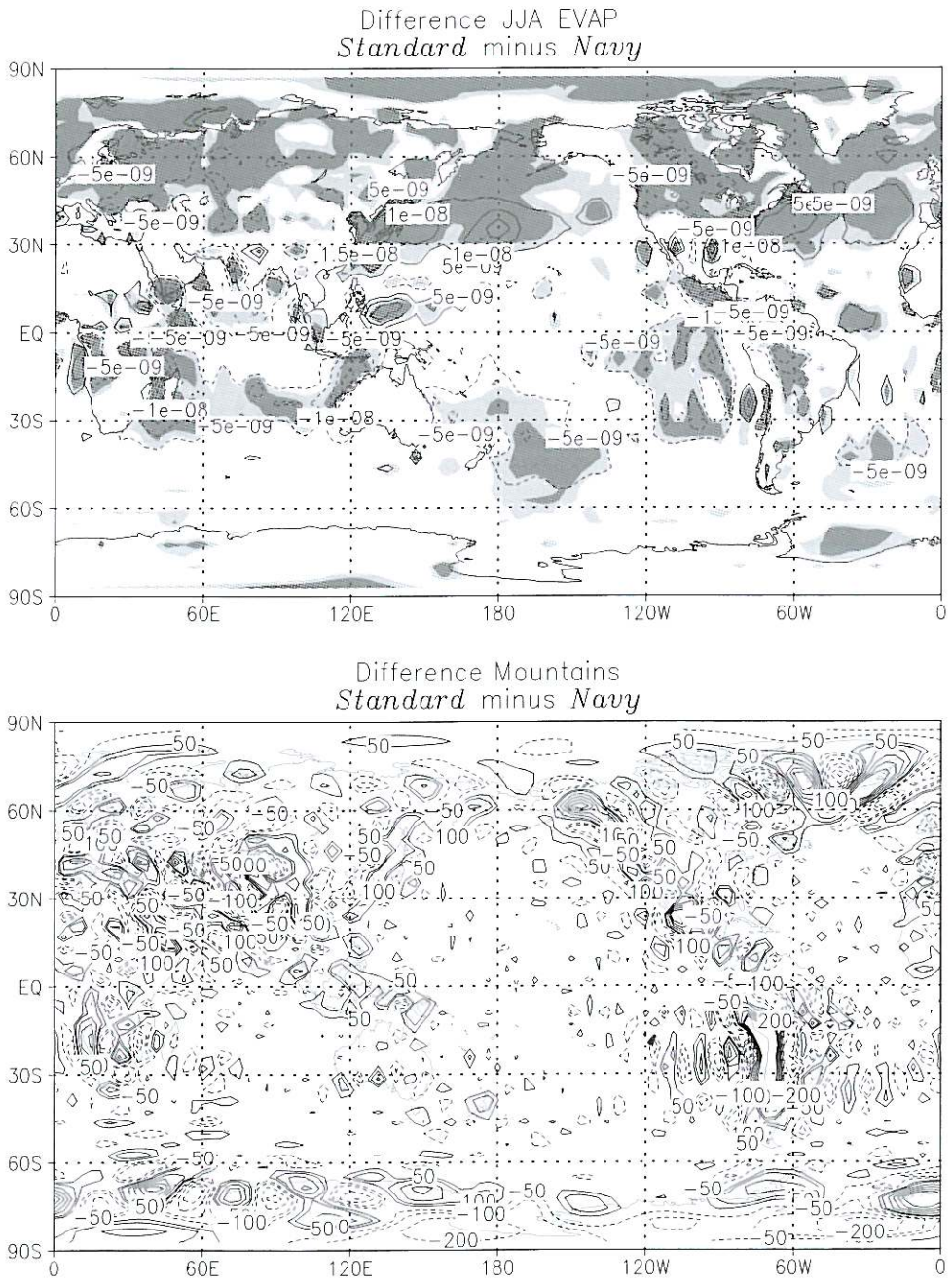

Fig. 23. Differences of evaporation between the Standard and Navy experiments (top) compared to the differences in the topographies (bottom). Areas significant at 5% and 1% are shaded and the contour in the top panel is kg/m^2 s and every 100 m plus the contours at 50 m and −50 m in the bottom panel.

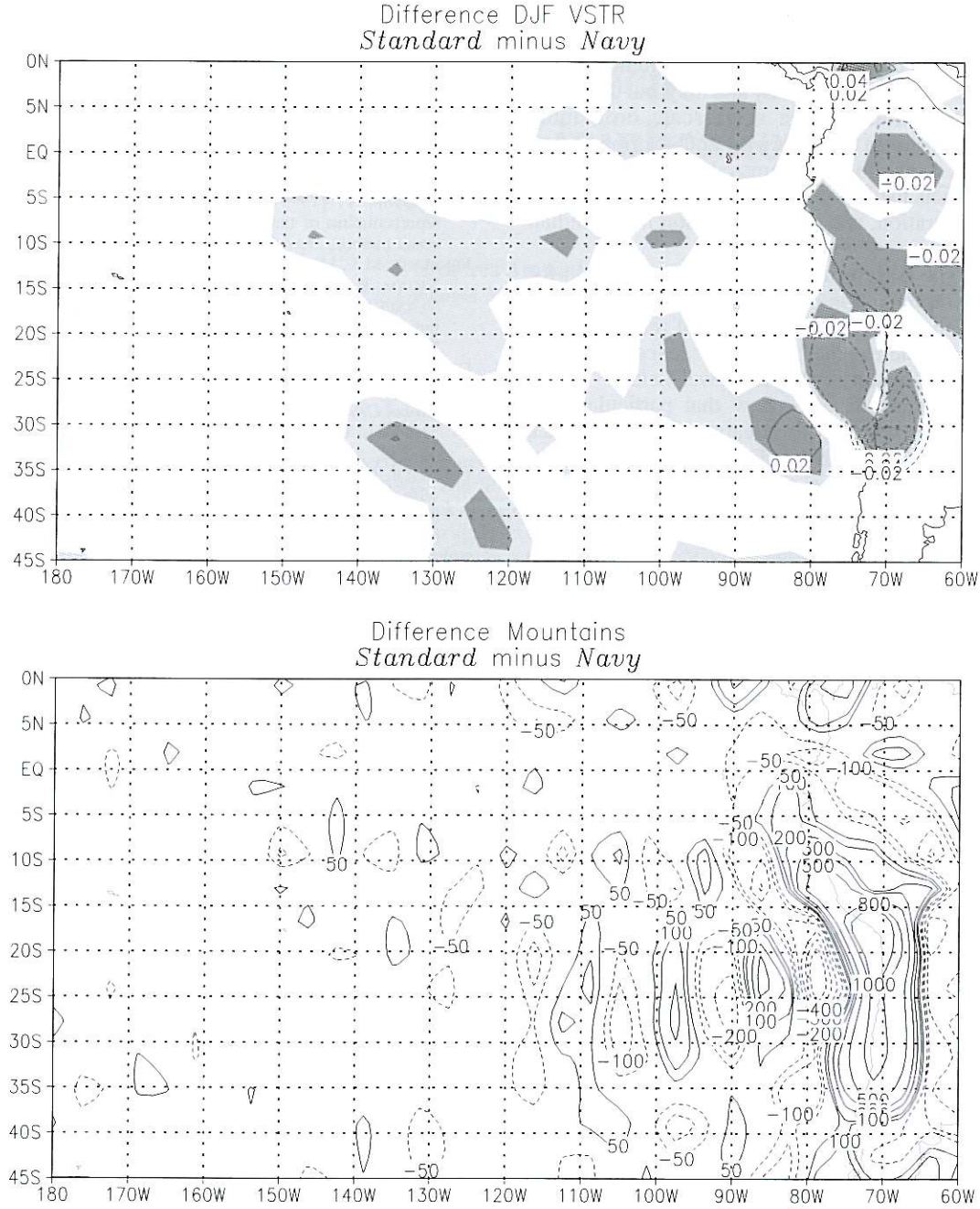

Fig. 24. Difference for winter (DJF) meridional wind stress field between the Standard experiment (011-AMIP) and the Navy mountains data set (021). Significance levels at 5% and 1% are shaded. The contour is 0.2 m in the top panel and at −400, −300, −200, −100, −50, 50, 100, 200, 300, 500, 800, 1000 m in the bottom panel.

numerical experiments show that the general circulation shows a marked sensitivity. The differences in the data sets contributes to the large scale upper air eddy anomaly, but the smaller amplitude of the small-scale orographic variability in both «Navy» and «Scripps» data sets, including the removal of Gibbs waves, impacts the low level local fields, especially the evaporation, and the precipitation in the Indian Ocean.

The Scripps data set gives the best result for the reproduction of the eddy anomalies, resulting in a substantial reduction of the systematic error, whereas the Navy data set seems to offer the best result for the low level fields.

The results also show that particular care must be taken in the treatment of the surface fields in the Southern Eastern Pacific. The observations show a meridional jet close to the coast that contributes significantly to the generation of the coastal upwelling that is a component of the ENSO dynamics in the equatorial area, slightly to the north. However, the Standard model generates a jet that is too spread out and displaced by about 500 km from the correct position in the open Pacific ocean. The filtered Navy mountains tend to produce a response in the right direction, *i.e.* shifting the jet toward the American coast. The effect is barely visible in the experiments, but it may represent an indication that there is a potential sensitivity in the area. This issue is potentially of great importance in the context of coupling the model to an ocean model to the effect of generating the right feedback between ocean and atmosphere. It is in fact clear that a systematic shift in the placement of the coastal jet could generate a rather large systematic response error, leading to the eventual absence of any upwelling. The models and the mountain representation should be carefully checked, and Gibbs waves and weak gradients eliminated, for this kind of systematic bias before coupling with ocean models.

Acknowledgements

This work was performed with the partial support of the EU program ENVIRONMENT under the project «Medium Term Climate Variability» (EV5V-CT92-0121). One of the authors (A. Navarra) would like to thank the wonderful hospitality and the generous support of the MPI, Hamburg, during several visits.

REFERENCES

BOUTELOUP, Y. (1995): Improvement of the spectral representation of the earth topography with a variational method, *Mon. Weather Rev.*, **122**, 1560-1573.

FENNESSY, M.J., J.L. KINTER III, B. KIRTMAN, L. MARX, S. NIGAM, E. SCHNEIDER, J. SHUKLA, D. STRAUS, A. VERNEKAR, Y. XUE and J. ZHOU (1994): The simulated Indian monsoon: a GCM sensitivitiy study, *J. Climate*, **7**, 33-45.

GATES, W.L. and A.B. NELSON (1975): *A New (Revised) Tabulation of the Scripps Topography on a 1 Degree Global Grid, part I: Terrain Heights.*, *R-1276-1-ARPA*, The Rand Corporation, Santa Monica, CA, U.S.A., pp. 132.

GOTTLIEB, D. and E. TADMOR (1985): Recovering pointwise values of discontinuous data within spectral accuracy, progress and supercomputing in computational fluid dynamics, in *Proceedings of the U.S. - Israel Workshop, 1984*, edited by EARLL M. MURMAN and SAUL S. ABARBANEL (Birkhauser, Boston, Basel, Stuttgart), 357-375

HOLZER, M. (1996): Optimal spectral topography and its effect on model climate, *J. Climate*, **9**, 2443-2463.

HOSKINS, B.J. (1980): Representation of the earth topography using spherical harmonics, *Mon. Weather Rev.*, **108**, 111-115.

JOSEPH, D. (1980): Navy 10′ global elevation values, *NCAR Research Notes on the FNWC Terrain Data Set*, pp. 3 [Available from NCAR Scientific Computing Division, Data Support Section, P.O. Box 3000, Boulder, CO 80307, U.S.A.].

NAVARRA, A., W.F. STERN and K. MIYAKODA (1994): Reduction of the Gibbs oscillations in spectral model simulations, *J. Climate*, **7**, 1169-1183.

ROECKNER, E., K. ARPE, L. BENGTSSON, M. CHRISTOPH, M. CLOUSSEN, L. DUMENIL, M. ESCH, M. GIORGETTA, U. SCHLESE and U. SCHULZWEIDA (1996): *The Atmospheric General Circulation Model ECHAM-4: Model Description and Simulation of Present-Day Climate*, Report No. 218, Max-Planck-Institut für Meteorologie, Hamburg, p. 86.

SCHUBERT, S., C.-K. PARK, W. HIGGINS, S. MOORTHI and M. SUAREZ (1990): An atlas of ECMWF analyses (1980-87). Part I - First moment quantities, *NASA Technical Memorandum 100747*, Goddard Space Flight Center, Greenbelt, MD, pp. 258.

WALLACE, J.M., S. TIBALDI and A.J. SIMMONS (1983): Reduction of systematic forecast errors in the ECMWF model through the introduction of an envelope topography, *Q. J. R. Meteorol. Soc.*, **109**, 683-718.

(received December 15, 1999;
accepted March 31, 2000)